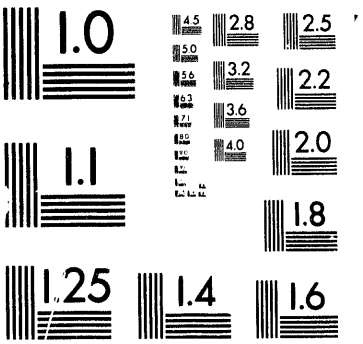
1.0
1.1
1.25
1.4
1.6
1.8
2.0
2.2
2.5
2.8
3.2
3.6
4.0
4.5
5.0
5.6
6.3
7.1
8.0
9.0

1 of 1

CONF-940222--7

WSRC-MS-93-518

CORRISION OF STEEL IN SIMULATED NUCLEAR WASTE SOLUTIONS

by
J. I. Mickalonis

Savannah River Site
Aiken, South Carolina 29808

DEC 09 1993
OSTI

A document prepared for:
Corrosion 94
at Baltimore, MD USA
from 2-28-94 thru 3-4-94

DOE Contract No. **DE-AC09-89SR18035**

This paper was prepared in connection with work done under the above contract number with the U. S. Department of Energy. By acceptance of this paper, the publisher and/or recipient acknowledges the U. S. Government's right to retain a nonexclusive, royalty-free license in and to any copyright covering this paper, along with the right to reproduce and to authorize others to reproduce all or part of the copyrighted paper.

MASTER

DISTRIBUTION OF THIS DOCUMENT IS UNLIMITED

DISCLAIMER

This report was prepared as an account of work sponsored by an agency of the United States Government. Neither the United States Government nor any agency thereof, nor any of their employees, makes any warranty, express or implied, or assumes any legal liability or responsibility for the accuracy, completeness, or usefulness of any information, apparatus, product, or process disclosed, or represents that its use would not infringe privately owned rights. Reference herein to any specific commercial product, process, or service by trade name, trademark, manufacturer, or otherwise does not necessarily constitute or imply its endorsement, recommendation, or favoring by the United States Government or any agency thereof. The views and opinions of authors expressed herein do not necessarily state or reflect those of the United States Government or any agency thereof.

This report has been reproduced directly from the best available copy.

Available to DOE and DOE contractors from the Office of Scientific and Technical Information, P. O. Box 62, Oak Ridge, TN 37831; prices available from (615) 576-8401.

Available to the public from the National Technical Information Service. U. S. Department of Commerce, 5285 Port Royal Rd., Springfield, VA 22161

CORROSION OF STEEL IN SIMULATED NUCLEAR WASTE SOLUTIONS

J. I. Mickalonis
Westinghouse Savannah River Company
Savannah River Technology Center
Aiken, SC 29841

ABSTRACT

Processing of inhibited nuclear waste to forms for long-term storage will cause waste tank environments to have dynamic conditions. During processing compositional changes in the waste may produce a corrosive environment for the plain carbon steel tanks. Large concentrations of nitrates which corrode steel are contained in the waste. Nitrite and hydroxides are added to inhibit any corrosion. Concentration changes of nitrate and nitrite were investigated to identify corrosion regimes that may occur during processing.

Corrosion testing was performed with cyclic potentiodynamic polarization and linear polarization resistance. Test samples were plain carbon steel which was similar to the material of construction of the waste tanks. The corrosion morphology of test samples was investigated by visual evaluation and scanning electron microscopy. Qualitative chemical analysis was also performed using energy dispersive spectroscopy.

The corrosion mechanism changed as a function of the nitrate concentration. As the nitrate concentration was increased the steel transitioned from a passive state to general attack, and finally pitting and crevice corrosion. The nitrate anion appeared to destabilize the surface oxide. Nitrite countered the oxide breakdown, although the exact mechanism was not determined.

Keywords: nuclear waste, nitrate, nitrite, inhibition, pitting

INTRODUCTION

Waste that was generated from the production of nuclear material will be processed to a stable form for long term storage. At the Savannah River Site (SRS) of the U.S. Department of Energy initial processing will occur in waste tanks where the waste is presently stored. The tank environments, therefore, will change from static storage conditions to dynamic processing conditions. This change may cause corrosive conditions in localized areas of the tanks. These conditions could be identified with corrosion monitoring, but the monitoring techniques must be adapted and developed for application to nuclear waste tanks.

An investigation was conducted at SRS to develop baseline data on the effect of changes in waste chemistry on corrosion processes of a waste tank. These data will support future corrosion monitoring activities. The laboratory tests were performed in concentrated salt solutions which simulated waste compositions. The wastes are composed primarily of nitrate salts and are inhibited with nitrite and hydroxide to prevent corrosion of the carbon steel tanks. The concentrations of these inhibitors were previously determined for nitrate concentrations that are anticipated for the different waste processes[1]. In this study, the nitrate and nitrite concentrations of simulated wastes were changed to obtain inhibitive and corrosive conditions. Standard electrochemical techniques and metallographic evaluation were used to evaluate these conditions.

EXPERIMENTAL PROCEDURE

Sample Preparation

The test samples were made from ASTM A537 plain carbon steel which is the material of construction of the most recent waste tanks at SRS. The nominal composition of this steel alloy is 0.24 %C, 0.70-1.60 %Mn, 0.040 %S, 0.035 %P, and 0.15-0.50 %Si with small amounts of Cu, Cr, and Ni[2]. The samples were either a flat, circular disk or a cylindrical rod. The disks were used for cyclic potentiodynamic polarization (CPP) tests and linear polarization resistance (LPR) measurements. A rod, which was a standard polarization resistance probe, was only for LPR measurements. The samples were supplied by Metal Samples (Munford, AL).

The circular disks had diameters of 0.625 in. (1.588 cm) and a thickness of 0.125 in. (0.318 cm). The disks were punched from rolled sheet and were ground to a 600-grit surface finish prior to each test. The cylindrical rods had diameters of 0.188 in. (0.478 cm) and lengths of 1.250 in. (3.175 cm). The rods were machined from rolled plate. The as-received surface had a 600-grit finish which was not reground prior to testing.

Test Setup

The tests were performed in a Greene-type corrosion cell equipped with a gas inlet, graphite counter electrodes, thermometer, and a Ag/AgCl reference electrode. A heating mantle and temperature controller

were used to maintain a constant temperature. The disks were held in a Teflon™ holder with a knife-edge gasket that exposed a surface area of 1 cm^2 to the solution. The rod was screwed onto a longer stainless steel rod which was isolated from the solution with a glass sleeve. A Teflon™ gasket was placed between the sleeve and the top of the test rod. The rod had an exposed surface area of approximately 7 cm^2. The data was taken on an EG&G Princeton Applied Research (PAR) Model 273 Potentiostat which was controlled by a personal computer.

LPR

LPR measurements were performed during exposure of a rod and disk sample to the simulated waste. The corrosion potential (E_{corr}) of the samples were monitored during the test. The test length was 45 days for the disk and 70 days for the rod. The solution temperature was 40°C. For LPR the potential was scanned over a range of +/- 0.010 V versus E_{corr} at a rate of 0.6 V/hr. An initial transition in the current density of approximately 0.2 uA/cm^2 was observed for both samples. The potential scan range and the direction of the scan did not affect this initial current transient. These points were removed from the database prior to calculating the polarization resistance (R_p). The remaining data displayed the expected linear relationship between potential and current density.

CPP

CPP tests were performed only with disk samples. Tests were conducted at 40°C in approximately 500 mL of solution. The vapor space in the cell was purged with nitrogen gas. The disk was placed into the solution and allowed to stabilize for 30 minutes. The tests were initiated at a potential -0.050 V versus E_{corr}. The potential was ramped at 0.6 V/hr. The vertex potential was 0.8 V (versus Ag/AgCl) and the final potential was 0.2 V versus E_{corr}. The samples were removed at the end of the tests, rinsed with distilled water, and blown dry for subsequent evaluation. Two tests were performed for each waste composition.

Simulated Waste Solution

The corrosion tests were conducted in concentrated salt solutions which simulated the waste. The base composition is given in Table 1. For both LPR and CPP, the sodium nitrate and nitrite concentrations were varied to alter the corrosive conditions of the solutions. The nitrate and the nitrite concentrations were increased by the addition of a 5 M sodium nitrate solution and a 40 wt% sodium nitrite solution, respectively.

For LPR, the samples were placed initially into a solution of the base composition. During the test, the nitrate concentration was increased without adjusting the nitrite concentration, which increased the solution corrosivity. The nitrite concentration was increased at the end of the test to try to sufficiently inhibit the solution. The target concentrations are shown in Table 2 for the LPR tests. The nitrite addition was calculated from inhibitor limits determined from previous

experimental work.

CPP tests were conducted in solutions with compositions similar to the LPR target compositions. Table 3 lists the actual nitrate and nitrite concentrations, as well as the pH of the solutions. These solutions will be referenced in this paper by their lettered designation given in the table. The solutions were made by adjusting the base composition, following the procedure for the LPR tests.

Metallurgical Evaluation

The test samples were examined with and without corrosion products using a stereomicroscope. They were cleaned according to ASTM G 1-88, "Standard Practice for Preparing, Cleaning, and Evaluating Corrosion Test Specimens". Scanning electron microscopy (SEM) with energy dispersive spectroscopy (EDS) was used to characterize the corrosion processes and to identify elemental compositions of corrosion products and the base material.

RESULTS

The test results from both CPP and LPR showed that the corrosivity of the simulated waste increased with the nitrate concentration. The nitrite anion inhibited this corrosion by possibly stabilizing the steel oxide. The corrosion process changed from general attack to pitting and crevice corrosion with the increased solution corrosivity. The metallurgical evaluation supported these findings and highlighted the effect of inclusions on the corrosion process.

CPP

The purpose of the CPP tests was to characterize the effect of nitrate and nitrite on the corrosion and inhibition of plain carbon steel in simulated waste. These tests were performed in five different solutions with different nitrate and nitrite concentrations. The polarization scans from these tests are shown in Figures 1-3. Table 4 lists E_{corr}, the passive current density (i_p), a critical potential (E_c), and a pit protection potential (E_{pp}) that were measured from the scans.

The nitrate concentration was increased for tests A, B, and C, which had similar nitrite concentrations. The nitrite concentration for test A was sufficient for inhibition. Tests D and E were performed to investigate the inhibitive action of nitrite. The nitrite concentration for test D was close to the limit for inhibition (0.208 M), although still below it. For test E the nitrite concentration was well above that necessary for inhibition (0.658 M).

The polarization scan for test A as shown in Figure 1 indicated that the steel was passive. Passivity initiated at a E_c of 0.17 V with a i_p of 0.3 uA/cm^2. The polarization characteristics changed as the nitrate concentration was increased for tests B and C. Figure 2 shows a representative polarization curve from these tests. The E_{corr} shifted to more active values and the i_p increased as shown by the values in Table 4. E_c resembled a pitting potential since at more noble potentials the

current density increased with the potential (i.e., i_p was not constant). The nitrate anion appeared to destabilize the oxide during formation at E_c, so the pitting resistance of the steel decreased.

Test D had a similar nitrate concentration to test B but a higher nitrite concentration, although insufficient for inhibition. The E_{corr} shifted to more active potentials than those for tests A-C. The i_p was similar to those for test B. A E_{pp}, however, was observed for one of the runs as shown by the polarization scan in Figure 3. The occurrence of E_{pp}, which was not observed in test B, was attributed to an increased inhibition of the higher nitrite concentration. The test results for test D indicated the borderline conditions for inhibition.

The nitrite concentration for test E was expected to be sufficient for inhibition at the greater nitrate concentration. The polarization curves from these tests were similar to that shown in Figure 3. The low and constant value of the i_p indicated a sufficient nitrite concentration was present for inhibition. The higher nitrate concentration, however, eventually caused pitting as evidenced by a hysteresis loop.

The results from test E were expected to be similar to those of test A since both nitrite concentrations were sufficient for inhibition. The results, however, showed that the test E solution was more corrosive. A contributing factor was the solution pH. In several additional tests, the pH of test solution A was adjusted to that for test E by the addition of a dilute nitric acid solution. The results indicated that the lower pH shifted E_{corr} to more electronegative values and i_p to larger average values, although the shift did not account for the total changes observed between tests A and E. The higher nitrate concentration of the test E solution also contributed to its increased corrosivity.

LPR

LPR test were conducted with a disk and a rod. The results differed slightly although both samples corroded in the higher nitrate solutions. The polarization resistance (R_p) and E_{corr} are shown graphically in Figures 4 and 5 for the disk and rod, respectively. The nitrate additions are indicated along the bottom of the graphs.

For the disk, the increased corrosivity at higher nitrate concentrations was indicated by a decrease in R_p and a shift in E_{corr} to more active values. During the initial ten-day period the sample was allowed to stabilize. The E_{corr} was stable at approximately 0.09 V; however, R_p was more variable. Discounting the initial transition, an average value of 50 kohms/cm was obtained. The changes in E_{corr} and R_p did not correlate well with the additions of nitrate to the solution. This result may have been from the short test period with frequent disturbances of the solution. By the end of the test, however, E_{corr} had shifted to potentials in the range of -0.1 to -0.2 V and the average R_p was 25 kohm/cm.

The test for the rod was longer with fewer nitrate additions. During the first 30 days, E_{corr} stabilized at approximately 0.04 V and R_p

increased to approximately 200 kohm/cm. The first nitrate addition was increased to minimize the frequent additions in the test for the disk. E_{corr} was not affected by this change, but R_p dropped to approximately 125 kohm/cm. At each subsequent nitrate addition E_{corr} was not affected, but R_p decreased to a final value of 40-50 kohm/cm. The addition of nitrite at the end of the test, which was to inhibit the solution, did not affect either E_{corr} or R_p.

The general trends of R_p for the disk and rod were similar, decreasing with increasing nitrate concentration. The trends in E_{corr} differed, although the initial potentials were similar. The disk potential became more electronegative, while for the rod E_{corr} remained fairly constant. The difference may be due to a surface area or geometric effect. A small amount of pitting will cause a smaller change in the potential of a larger sample. From qualitative observations of the surface as discussed below, the disk did appear to have a greater amount of corrosion. Another possible factor is the large interfacial area between the disk sample and the holder than that for the rod. This area is susceptible to crevice corrosion which will cause E_{corr} to be more active.

Metallurgical Evaluation

A visual evaluation and microstructural and chemical analyses were used in this study to identify the corrosion morphology and to investigate correlations between the morphology and the microstructure of the sample. In general, pitting was the dominant corrosion process although crevice and general corrosion also occurred. Various initiation sites for pitting were found and attributed to the initial surface condition and the underlying microstructure.

Microstructural Characterization Of Samples. The electrochemical disks and rod electrodes had different initial surface conditions and microstructures. The differences were attributed to the material processing and specimen preparation procedures. According to the supplier, the disks were machined from 1/8-in. plate and the rods were machined from 1/4-in. plate. The microstructure of the exposed surface depended on the orientation of the sample relative to the rolling direction of the plate.

For the disks, two different microstructures were observed as shown in the micrographs of Figure 6. Figure 6A shows a laminar microstructure of ferrite and pearlite found in the test samples from CPP. The disk that was used for LPR had a fairly uniform distribution of ferrite and pearlite as shown in Figure 6B. Both microstructures contained inclusions as shown in the SEM photomicrograph in Figure 7. The energy dispersive spectra, shown in Figure 8, had peaks for aluminum, sulfur, manganese, oxygen, and iron which indicated that the inclusions were aluminum oxides and manganese sulfides. The iron peak was attributed to the base steel.

The rod electrode had a laminar microstructure in the transverse and cross sectional directions, similar to that shown in Figure 6A. Aluminum oxide and manganese sulfide inclusions were also found. The

microstructure of the exposed surface of the rod was more complex since it varied around the circumference of the sample.

Both the rod and the disks were prepared to a 600-grit surface finish, but the rod had a coarser appearance. Gashes were present on the surface of the rod, but were not on that of the disk. The rod was prepared by the manufacturer, while the disks were prepared in the laboratory immediately prior to testing.

Corrosion Morphology Of CPP Disks. The samples in the base solution (test A), which was characterized as inhibitive, were fairly free of corrosion. A slight discoloration was observed, which may have resulted from the rinsing procedure after the test. The samples were not examined further.

The samples from test B had areas of general attack with a number of small pits (5-10 microns). These pits probably initiated either at exposed subsurface inclusions or in troughs that resulted from general attack. The pits were round or elliptical and many were associated with aluminum oxide or manganese sulfide inclusions. Some oxide inclusions also contained small amounts of magnesium and calcium. These particles may have come from the retention of slag. Many of the pits were in linear arrays as shown in the photomicrograph of Figure 9.

Crevice attack under the gasket was found on the B samples. The attack at grain boundaries in these regions was significant and may be associated with impurities. Pitting was also observed. The different polarization scans for the test B samples correlated with a varying amount of crevice corrosion.

Pitting was more significant on the test C samples. Pit widths were approximately 5-10 microns, but appeared deeper than those on test B samples. The pits had domes of corrosion products similar to those shown in Figure 10 for test E samples. The degradation of test C samples did not appear as severe as that observed on test B samples. The more extensive general attack on test B samples may have caused this anomaly. Some crevice corrosion at the gaskets was also observed on test C samples.

For test D samples, the corrosion morphologies differed which was indicated by their different polarization results. For the test results which indicated active corrosion, the sample pitted and corroded under the gasket. The other sample was pitted similar to test C samples. The D test samples were the first to be found with mercury particles on the surface, which are shown in Figure 11. Mercury deposition may have been an alternate cathodic reaction resulting from a shift in the sample potential.

Test E samples had pit morphologies similar to those of test D samples including the presence of mercury particles. Pitting of the test E samples did not appear significantly different from those of test D. Crevice corrosion at the gasket was also found on the test E samples.

Corrosion Morphology of LPR Samples. The morphology and extent of

corrosion differed for the disk and the rod. A macroscopic photograph of the test samples is shown in Figure 12. The corrosion of the disk was greater than that of the rod even though the test length for the disk was shorter. The differences in the corrosion may have been due to several factors. These factors include variation in solution chemistry, sample geometry, surface preparation, and sample microstructure. The corrosion on the disk was concentrated at the perimeter of the exposed area near the gasket region. The rod had a tarnished appearance with minimal corrosion products. Regions near the top of the rod were more severely attacked than those near the bottom, although this difference is not apparent in the figure.

The corrosion products on the disk had a crusty appearance with particulate matter of variable size as shown in Figure 13. EDS analysis revealed that the crusty regions were composed of iron and aluminum oxides. Sodium and sulfur species were also present. The larger particulates were primarily aluminum oxides with smaller amounts of potassium, calcium, magnesium, and silicon. The small white particles in the micrograph were composed of mercury and silver. The origin of the silver was unknown.

After the removal of corrosion products, pitting and general corrosion were found. Most of the pitting was associated with aluminum oxide and manganese sulfide inclusions as observed on the cyclic polarization samples. In several regions the grains appeared to be preferentially attacked as shown in Figure 14. If this attack revealed an inclusion, pitting appeared to be initiated. Some particles containing mercury and silver were still present even after cleaning.

The corrosion products on the rod were primarily iron oxides although aluminum and silicon were also detected. Cleaning the rod did not greatly change its appearance since only a minimal amount of corrosion product was present. Pitting was the prevalent corrosion mechanism. The pits did not have caps of corrosion products as observed on some of the cyclic polarization samples. The pits were found, however, to be in linear arrays and have either round or slightly elongated shapes. Some pits also initiated at surface gashes.

CONCLUSIONS

The corrosion of plain carbon steel in simulated waste solution depended on the nitrate and nitrite concentration. The degree and morphology of corrosion changed as the nitrate concentration increased or the nitrite concentration decreased (i.e., the corrosivity of the solution increased). Plain carbon steel was passive if the solution was sufficiently inhibited. As solution corrosivity increased, the corrosion process transitioned to general attack and then pitting. Crevice corrosion also occurred with increased corrosivity.

The pitting of plain carbon steel exposed to waste tank environments resulted from the nitrate anion which destabilized the oxide on the steel. The nitrite anion has the opposite effect although the exact mechanism is unknown. Metallographic analysis showed that pits nucleated primarily at manganese sulfide and aluminum oxide inclusions.

The inclusions were either at the surface or exposed after general corrosion. Pits may also be initiated at surface flaws.

The solution corrosivity was also correlated to R_p values; decreasing as the nitrate concentration was increased. These values will be used as a baseline data for the development of corrosion monitoring techniques for the waste tanks. The E_{corr} was not as sensitive to solution corrosivity, especially on the LPR probe. Although R_p values can not be used to detect the onset of pitting, monitoring of R_p in the waste tanks could be used as an indicator of the increased susceptibility of the waste tanks to corrosion.

ACKNOWLEDGEMENTS

The author wishes to thank Angela Lacey and Jack Durden for their assistance with the experimental work and Phil Zapp and Bruce Wiersma for helpful discussions.

REFERENCES

1. P. E. Zapp, D. T. Hobbs, "Inhibiting Pitting Corrosion In Carbon Steel Exposed To Dilute Radioactive Waste Slurries," CORROSION/92, paper no. 98, (Houston, TX: NACE, 1992).

2. G. J. Roe, Metals Handbook Ninth Edition: Volume 1 Properties and Selection: Iron And Steel (Metals Park, OH: American Society of Metals, 1978), p. 185.

TABLE 1
COMPOSITION OF SIMULATED ITP WASHED PRECIPITATE SOLUTION

Constituents	Concentration (M)
Aluminum Nitrate	2.05E-2
Iron Nitrate	5.50E-3
Sodium Hydroxide	9.37E-2
Sodium Nitrate	5.18E-3
Sodium Nitrite	2.57E-2
Sodium Oxalate	8.66E-3
Sodium Sulfate	5.94E-3
Sodium Carbonate	5.80E-2
Sodium Bicarbonate	1.20E-2
Sodium Hypophosph.	3.90E-4
Calcium Carbonate	6.60E-4
Sodium Chloride	1.03E-3
Sodium Fluoride	7.30E-4
Sodium Chromate	1.40E-4
Chromium Chloride	6.00E-5
Sodium Molybdate	1.85E-5
Sodium Metasilic.	1.60E-4
Uranyl Nitrate	3.30E-4
Cobalt Nitrate	1.50E-6
Copper Nitrate	2.00E-5
Manganese Dioxide	1.14E-3
Nickel Nitrate	5.20E-4
Mercury Nitrate	1.10E-4
Zinc Nitrate	4.00E-5
Lead Nitrate	2.00E-5
Phenol	4.30E-6

TABLE 2
NITRATE AND NITRITE CONCENTRATIONS FOR LPR MEASUREMENTS

Addition	Nitrate Concentration (M)	Nitrite Concentration (M)
0	0.022	0.030
1	0.037	0.03
2	0.0797	0.0297
3	0.184	0.029
4	0.298	0.028
5	0.704	0.026
6	0.64	1.086

TABLE 3
NITRATE AND NITRITE CONCENTRATIONS FOR CPP TESTS

Test	Nitrate Concentration (M)	Nitrite Concentration (M)	pH
A	0.022	0.030	9.46
B	0.184	0.029	9.34
C	0.310	0.028	9.27
D	0.181	0.161	9.25
E	0.549	0.946	9.00

TABLE 4
ELECTROCHEMICAL PITTING PARAMETERS FROM CPP TESTS

Test	E_{corr} (V Ag/AgCl)	i_p (uA/cm^2)	E_c (V Ag/AgCl)	E_{pp} (V Ag/AgCl)
A	0.050	0.3	0.17	--
	0.062	0.3	0.17	--
B	-0.129	3.2	0.17	--
	-0.132	3.2	0.17	--
C	-0.161	>10	0.17	--
	-0.124	>10	0.17	--
D	-0.175	3.2	0.17	--
	-0.243	1.0	0.17	0.575
E	-0.267	1.0	0.17	0.550
	-0.291	1.0	0.17	0.525

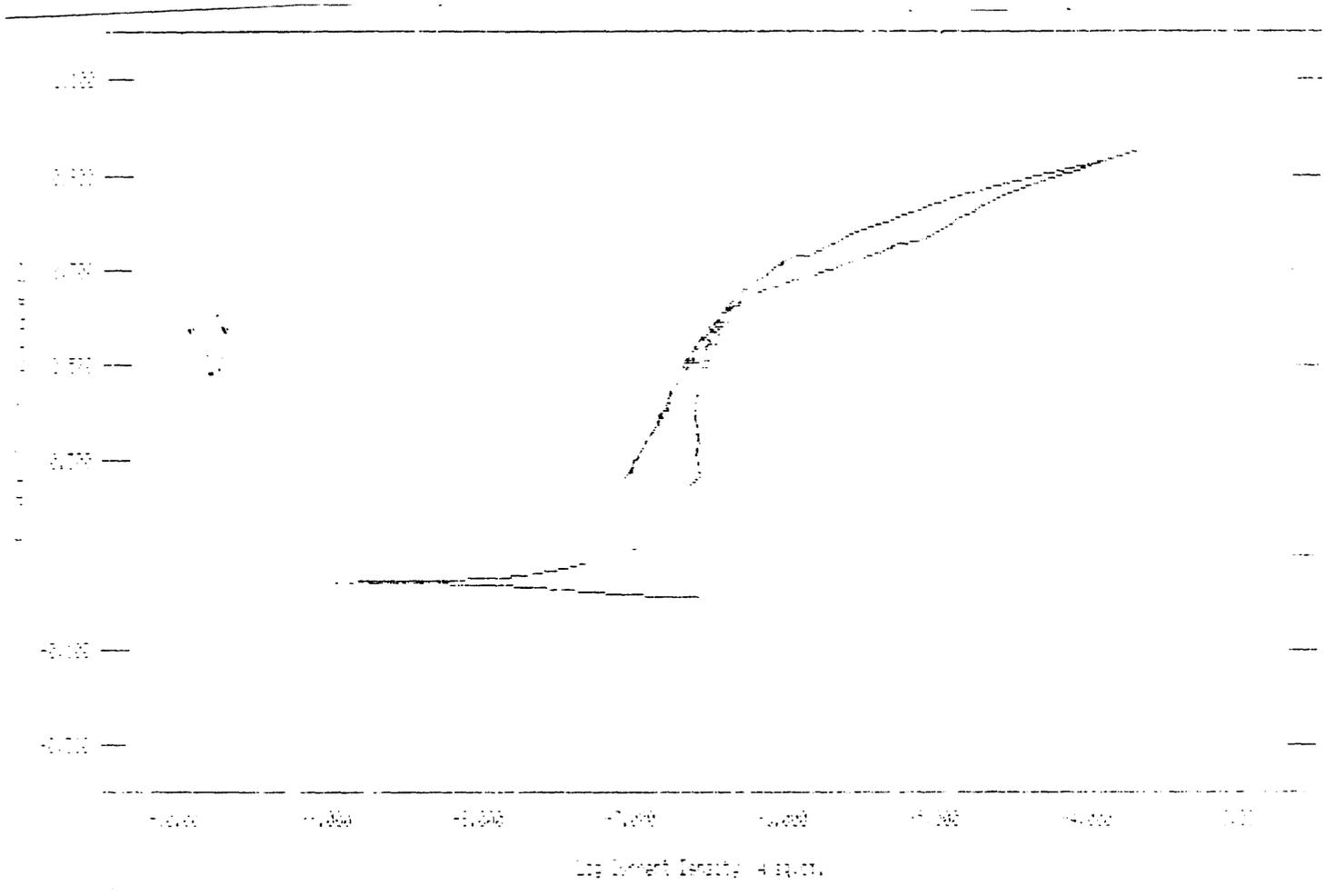

Figure 1. Polarization scan for A537 plain carbon steel in a simulated ITP washed precipitate solution with 0.022 M sodium nitrate and 0.031 M sodium nitrite (Test A)

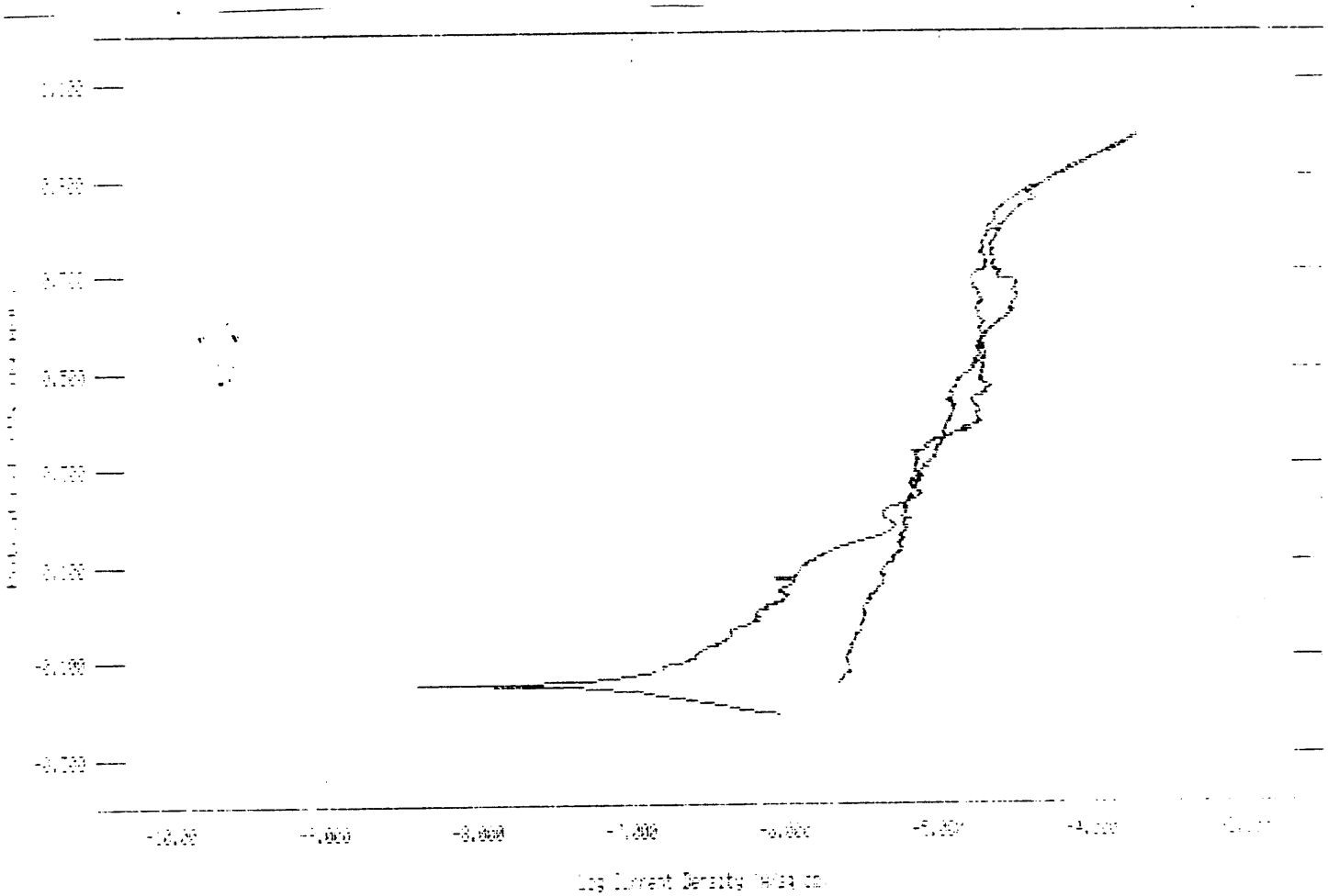

Figure 2. Polarization scan for A537 plain carbon steel in a simulated ITP washed precipitate solution with 0.310 M sodium nitrate and 0.028 M sodium nitrite (Test C)

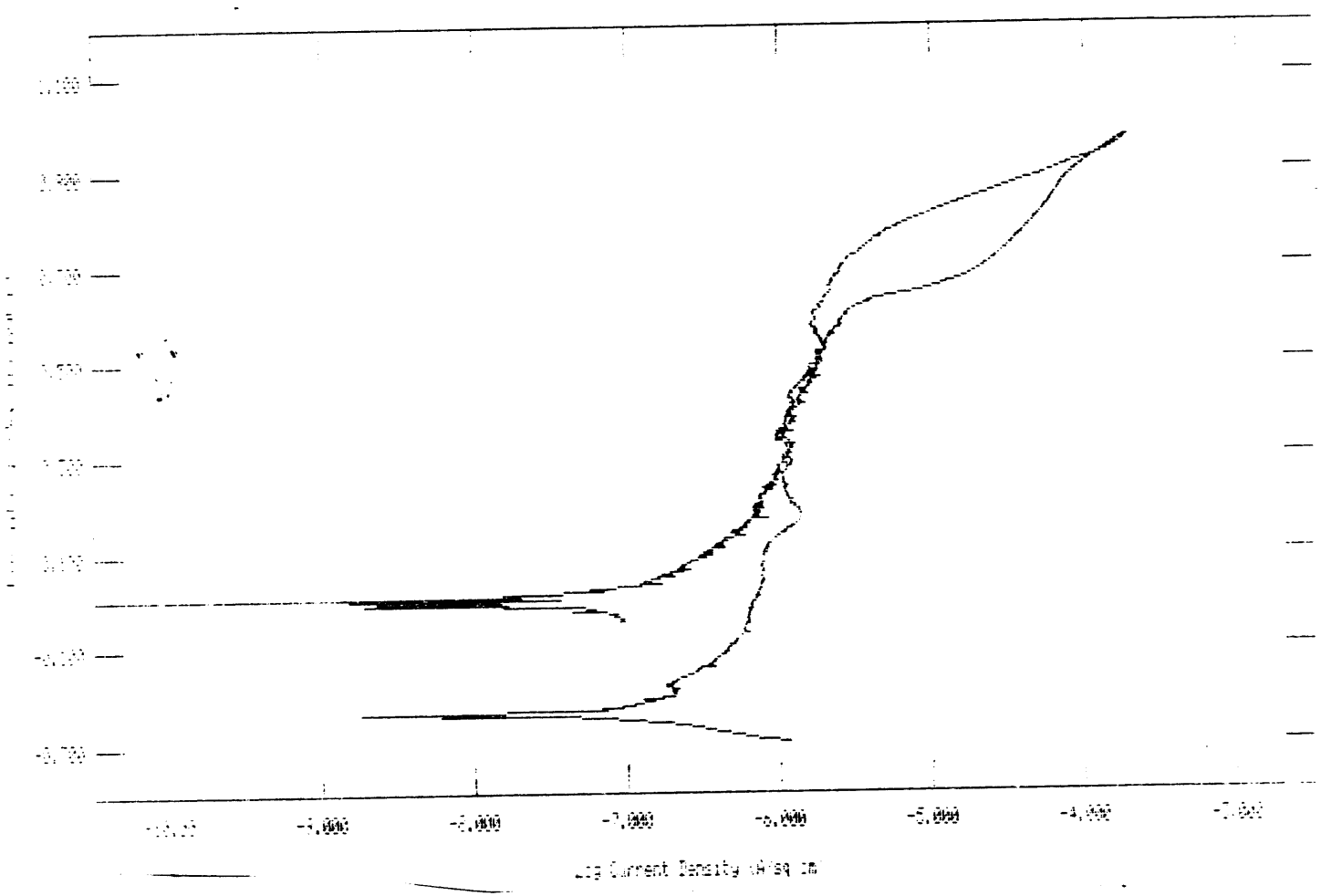

Figure 3. Polarization scan for A537 plain carbon steel in a simulated ITP washed precipitate solution with 0.181 M sodium nitrate and 0.161 M sodium nitrite (Test D)

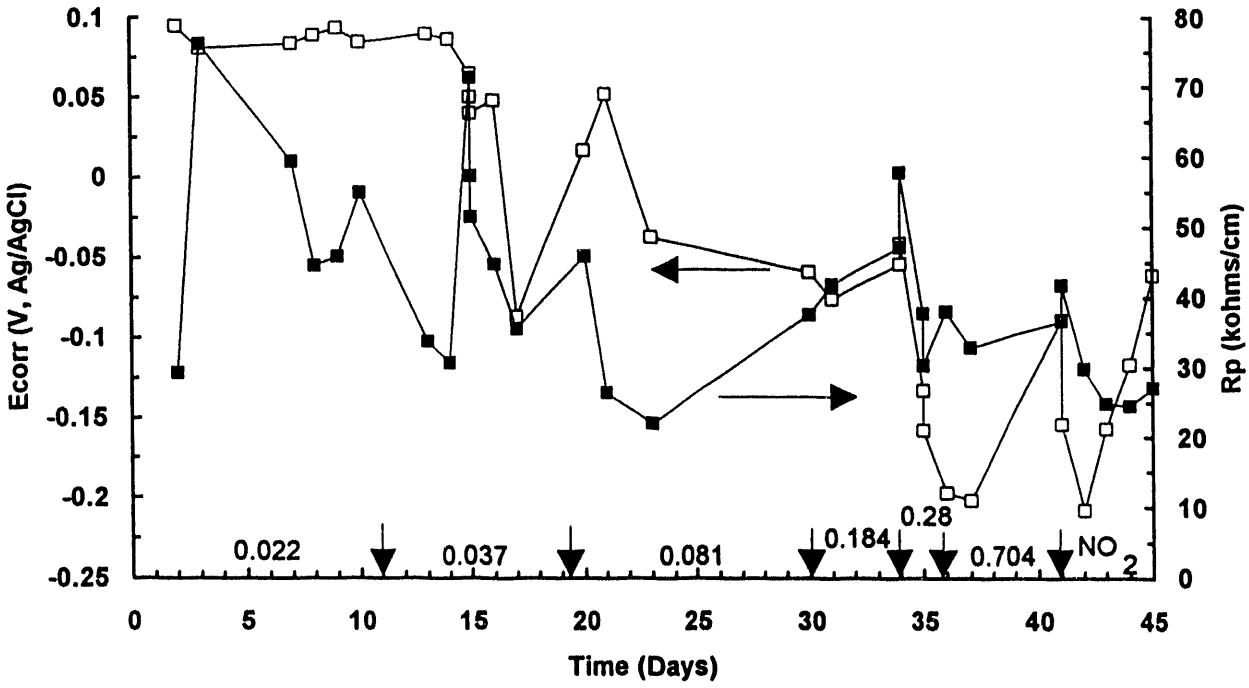

Figure 4. E_{corr} and R_p measurements with a disk sample of A537 plain carbon steel

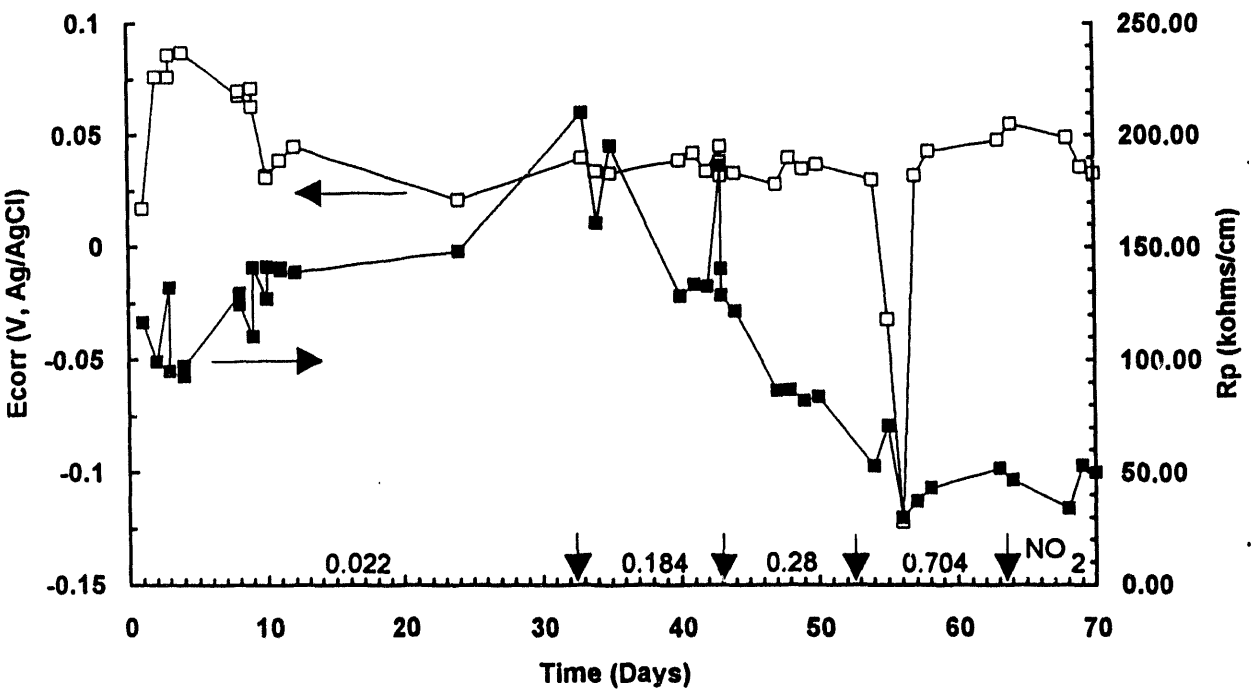

Figure 5. E_{corr} and R_p measurements with a rod sample of A537 plain carbon steel

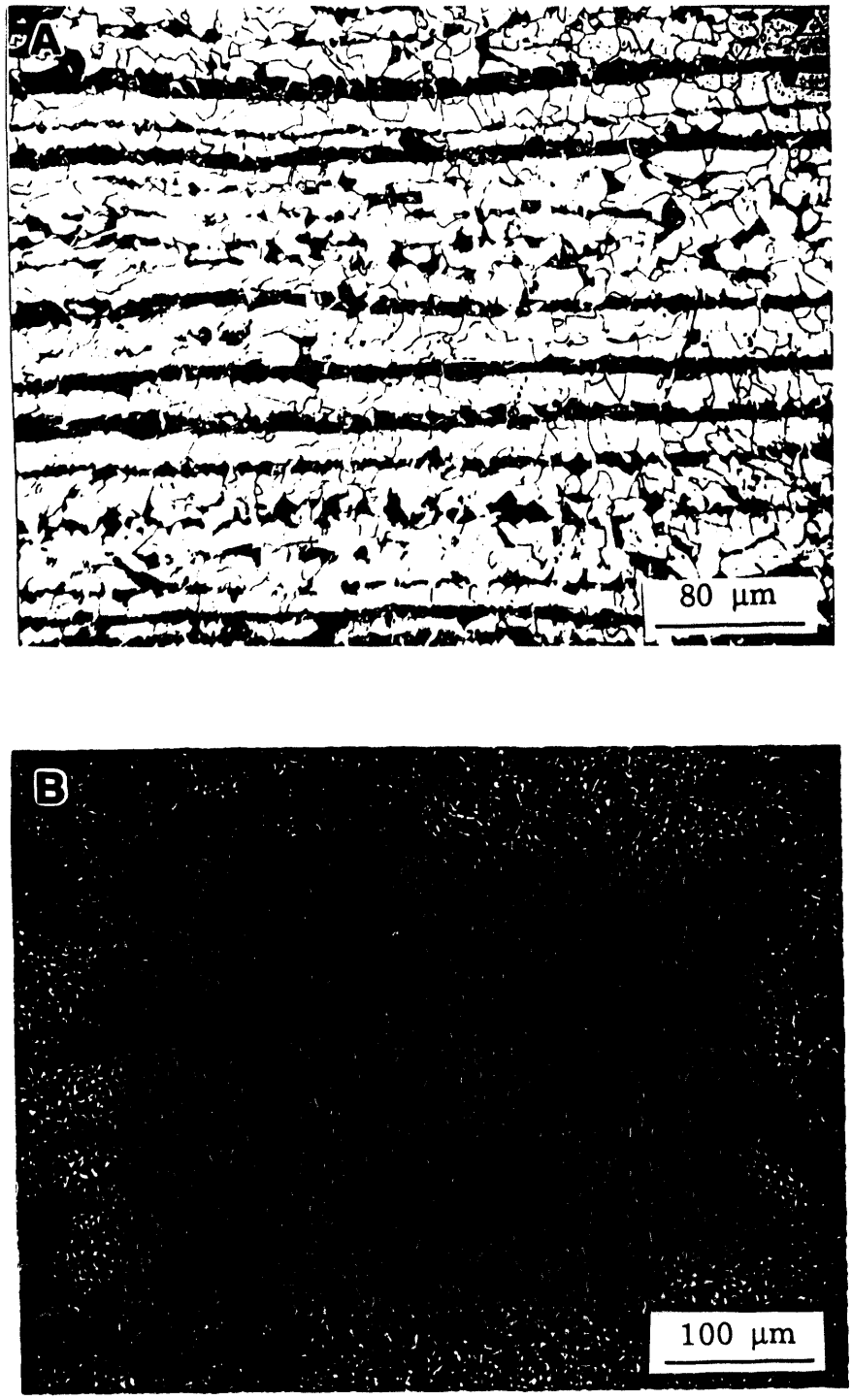

Figure 6. Microstructures of A537 plain carbon steel disks used for CPP and LPR: (A) laminar morphology of ferrite and pearlite, (B) uniform distribution of ferrite and pearlite

Figure 7. Surface inclusions in A537 plain carbon steel rod samples

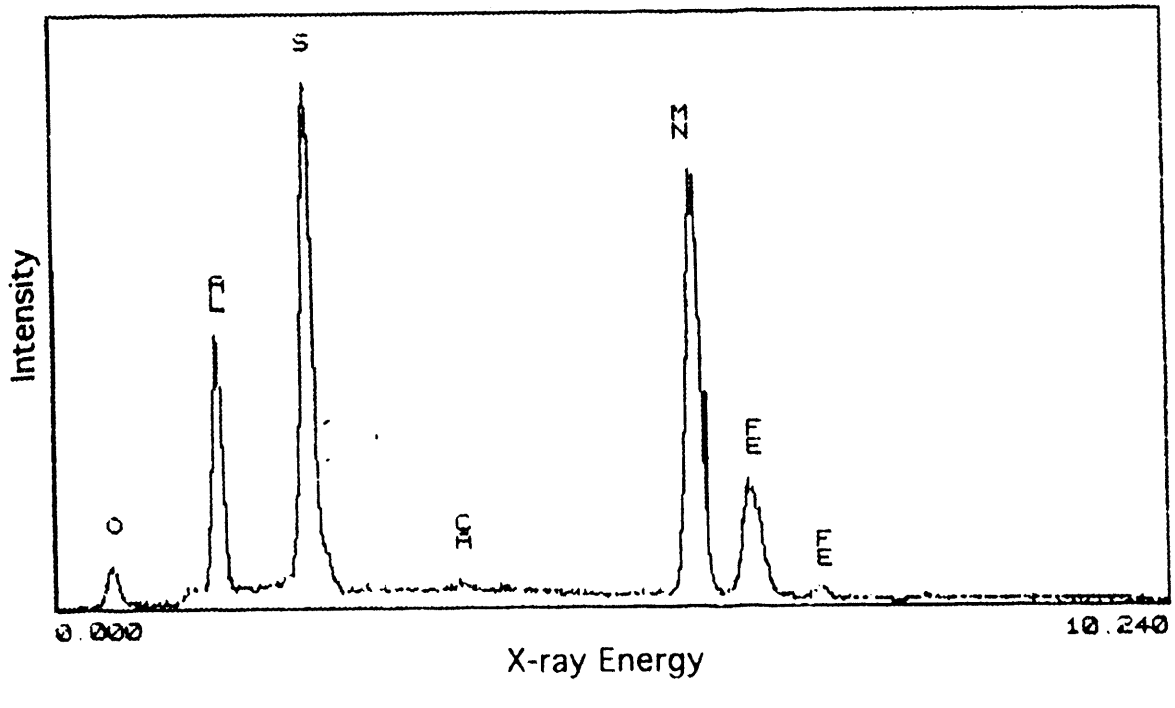

Figure 8. EDS spectra of inclusion shown in Figure 7

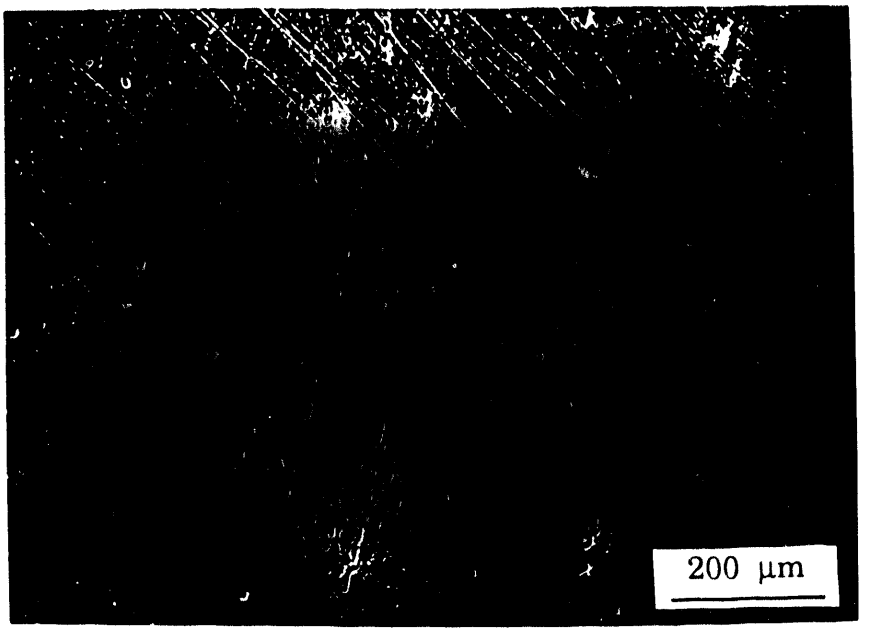

Figure 9. Linear array of pits on a disk sample from test B

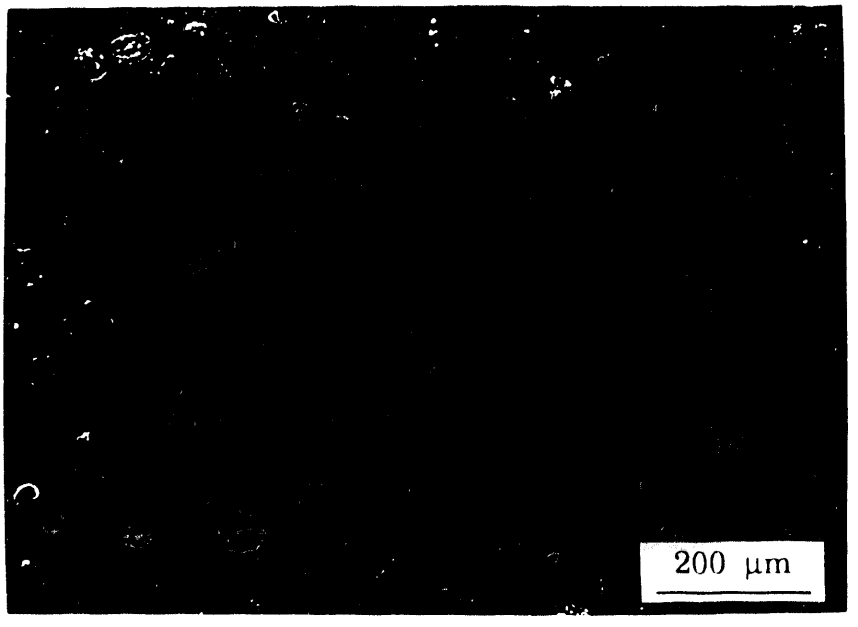

Figure 10. Corrosion pits covered with domes of corrosion products

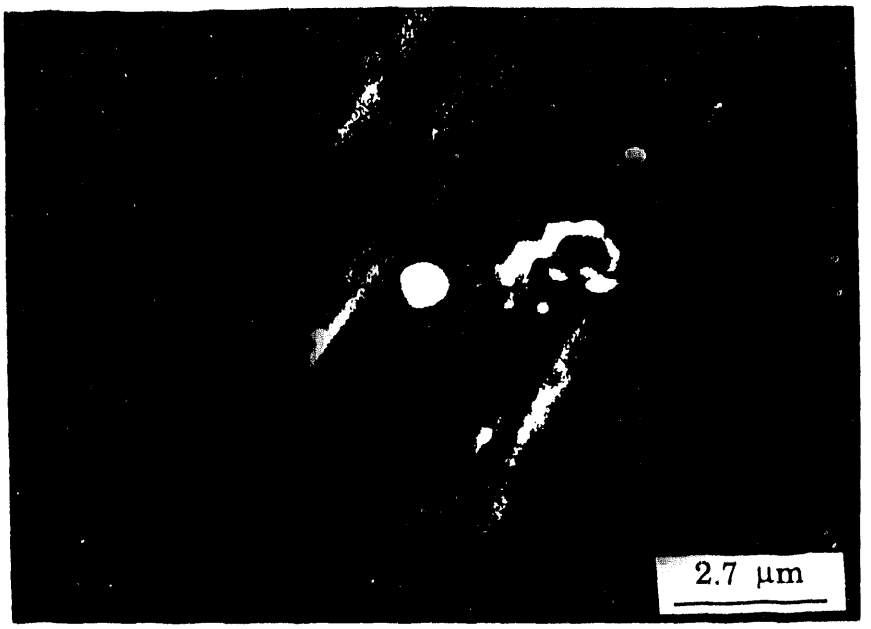

Figure 11. Mercury particle on a sample from test D

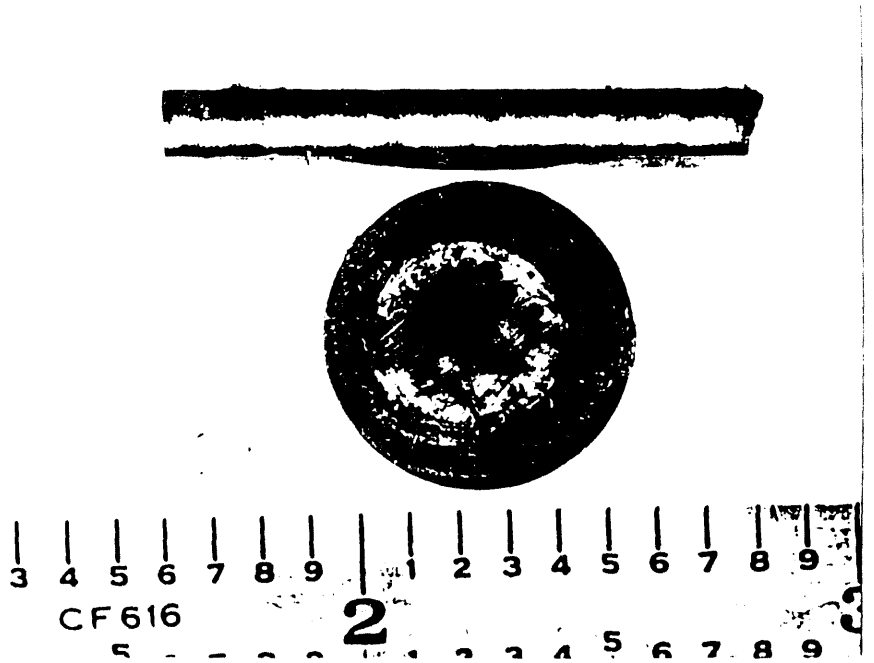

Figure 12. Rod and disk samples used for LPR measurements

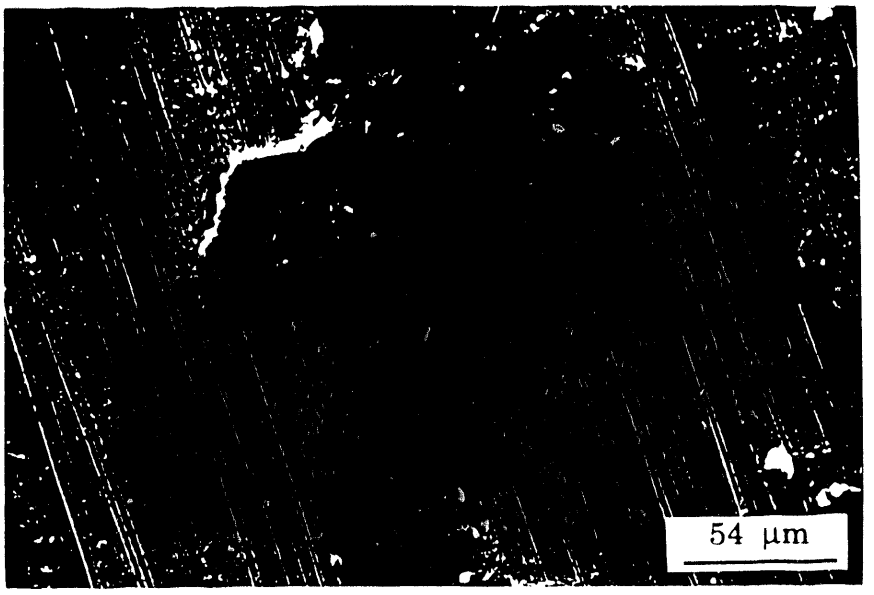

Figure 13. Corrosion products that formed on disk sample from LPR

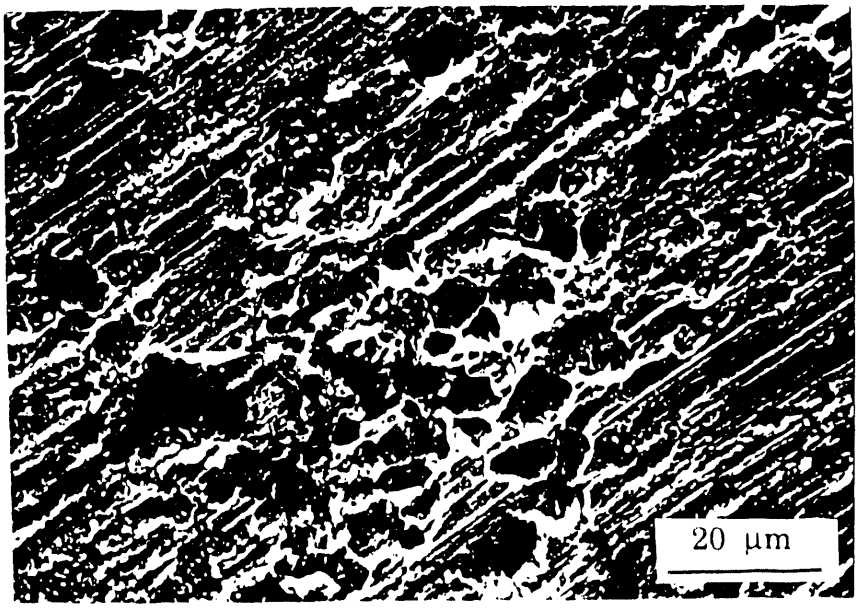

Figure 14. Preferential grain attack on the rod sample from LPR

DATE
FILMED
1/26/94
END